Mechanical Systems and Signal Processing 27 (2012) 712–728

Contents lists available at SciVerse ScienceDirect

Mechanical Systems and Signal Processing

journal homepage: www.elsevier.com/locate/ymssp

Multivariate EMD and full spectrum based condition monitoring for rotating machinery

Xiaomin Zhao, Tejas H. Patel, Ming J. Zuo*

University of Alberta, Edmonton, AB, Canada T6G 2G8

ARTICLE INFO

Article history:
Received 30 November 2010
Received in revised form
10 July 2011
Accepted 1 August 2011
Available online 26 August 2011

Keywords:
Condition monitoring
Multivariate EMD
Full spectrum
Mutual information

ABSTRACT

Early assessment of machinery health condition is of paramount importance today. A sensor network with sensors in multiple directions and locations is usually employed for monitoring the condition of rotating machinery. Extraction of health condition information from these sensors for effective fault detection and fault tracking is always challenging. Empirical mode decomposition (EMD) is an advanced signal processing technology that has been widely used for this purpose. Standard EMD has the limitation in that it works only for a single real-valued signal. When dealing with data from multiple sensors and multiple health conditions, standard EMD faces two problems. First, because of the local and self-adaptive nature of standard EMD, the decomposition of signals from different sources may not match in either number or frequency content. Second, it may not be possible to express the joint information between different sensors. The present study proposes a method of extracting fault information by employing multivariate EMD and full spectrum. Multivariate EMD can overcome the limitations of standard EMD when dealing with data from multiple sources. It is used to extract the intrinsic mode functions (IMFs) embedded in raw multivariate signals. A criterion based on mutual information is proposed for selecting a sensitive IMF. A full spectral feature is then extracted from the selected fault-sensitive IMF to capture the joint information between signals measured from two orthogonal directions. The proposed method is first explained using simple simulated data, and then is tested for the condition monitoring of rotating machinery applications. The effectiveness of the proposed method is demonstrated through monitoring damage on the vane trailing edge of an impeller and rotor-stator rub in an experimental rotor rig.

1. Introduction

Condition monitoring is of fundamental importance for the safe operation of rotating machinery. By checking the machine health condition, proper maintenance could be scheduled, thus avoiding the consequences of failure. Vibration analysis is extremely important for successful machinery condition monitoring. Depending upon the fault type, vibration in one or more directions becomes significant. Moreover, the location of a fault and its structural path greatly influence the quality of a measured vibration signal. For this reason, a set of vibration sensors are usually involved in the condition monitoring process [1].

In condition monitoring of rotating machinery, utilizing advanced signal processing techniques for analyzing vibration signals and extracting fault features has become very popular in the last decade or so. Techniques such as the wavelet

* Corresponding author. Tel.: +1 780 492 4466; fax: +1 780 492 2200.
E-mail address: ming.zuo@ualberta.ca (M.J. Zuo).

0888-3270/$ - see front matter © 2011 Elsevier Ltd. All rights reserved.
doi:10.1016/j.ymssp.2011.08.001

transform (WT) [2], empirical mode decomposition (EMD) [3], Hilbert – Huang transform [4] and their variants are widely used for this purpose. In wavelet transform, a signal is represented by wavelet coefficients through conjunction with wavelet basis. The results of this analysis are thus affected by the choice of wavelet basis; this may lead to a subjective prior assumption regarding the characteristics of the investigated signal. The EMD, on the other hand, is a self-adaptive technique. It decomposes a raw signal into a set of complete and almost orthogonal components called intrinsic mode functions (IMFs). IMFs represent the natural oscillatory modes embedded in the raw signal. They work as the basis functions which are determined by the raw signal rather than by pre-determined functions. Therefore, EMD has been widely used for fault diagnosis of rotating machinery [5,6]. However, standard EMD algorithm [7] is designed to process real-valued data only. Signals from multiple sensors and/or from different health conditions are processed individually, and fault features are extracted from each individual set of IMFs [3–5]. There are two problems associated with extracting fault features in this way. First, because of the local and data-driven nature of EMD, there is no guarantee that the decomposition results of signals from different sources will match [8], either in number or their properties (i.e. frequency content); this makes a multi-scale comparison between different damage conditions difficult. Second, the joint information between multiple sensors is not considered because signals from multiple sensors are treated individually.

To ensure proper decomposition of signals from different sources, standard EMD has recently been extended to the multivariate versions of EMD including those suitable for the bivariate signals [9], trivariate signals [10] and multivariate signals [11]. Bivariate EMD [9] estimates the local mean by mapping a bivariate signal to a number of real-valued projected signals and averaging the local mean of these projected signals. Bivariate EMD is employed to facilitate the synchronization of image fusion [8] and to diagnose a fault of a rotor [12]. Following the same idea, trivariate EMD [10] is proposed for three-dimensional signals. Multivariate EMD [11] further generalizes this concept for n-dimensional signals.

Joint information between sensors can provide important information on the health condition of machinery, e.g. the phase information between two orthogonal sensors [13,14]. Assessing signals obtained from the multiple sensors is helpful for efficiently extracting fault information; therefore it is gaining more and more attention in the recent past. Baydar et al. [15] introduced the application of multivariate statistical process control to successfully detect tooth defects. Ge et al. [1] developed two statistics-based techniques for monitoring mechanical systems that produce stochastic, non-Gaussian, and correlated vibration signals. However, these statistics-based methods rely on principal component analysis (PCA), independent component analysis (ICA) and their extensions [1,15]. The physical meaning of the raw signals was lost as a result of the linear or non-linear transformations involved in the statistical methods. Full spectrum is a signal-based technique which deals with two orthogonal signals and reveals the directivity of a vibration motion with respect to the rotational direction. This gives full spectrum great potential for the condition monitoring of rotating machinery [13,14,16,17].

In this paper, we propose a method of extracting a feature from multiple sensors for the condition monitoring of rotating machinery. The proposed method combines the advantages of multivariate EMD and full spectrum, using the mutual information theory to identify a unique IMF. A feature extracted from this unique IMF helps to detect faults and their severity. The rest of the paper proceeds as follows. Sections 2 and 3 give brief introductions to multivariate EMD and full spectrum. Section 4 describes the procedure for the proposed method. Section 5 applies the proposed method to both simulated data and experimental data obtained from a centrifugal pump and an experimental rotor test-rig. Conclusions come in Section 6.

2. Multivariate empirical mode decomposition (multivariate EMD)

2.1. Standard EMD [7]

For a real-valued signal, $x(t)$, standard EMD finds a set of IMFs, $c_i(t)$, and a residual signal, $r(t)$, so that

$$x(t) = \sum_{i=1}^{N} c_i(t) + r(t) \tag{1}$$

The IMFs are defined so as to have symmetric upper and lower envelopes with the number of zero crossings and the number of extrema differing at most by one. To extract IMFs, an iterative process called sifting algorithm is employed, which is described below.

Step 1: Find the locations of all the extrema of $x(t)$.
Step 2: Interpolate between all the minima to obtain the lower signal envelope, $e_{min}(t)$. Interpolate between all the maxima to obtain the upper signal envelope, $e_{max}(t)$.
Step 3: Compute the local mean, $m(t) = [e_{min}(t) + e_{max}(t)]/2$.
Step 4: Subtract the mean from $x(t)$ to obtain the "oscillatory mode", $s(t) = x(t) - m(t)$.
Step 5: If $s(t)$ satisfies the stopping criteria, then define $c_1(t) = s(t)$ as the first IMF; otherwise, set new $x(t) = s(t)$ and repeat the process from Step 1.

The same procedure is applied iteratively to the residue, $r(t) = x(t) - c_1(t)$, to extract other IMFs. The standard stopping criterion terminates the shifting process when the defined conditions for an IMF is met S consecutive times [18].

2.2. Multivariate EMD

Standard EMD considers only one-dimensional signals and the local mean is calculated by averaging the upper and lower envelopes (obtained by interpolating between the local maxima and minima, respectively). For multivariate signals, however, the local maxima and minima cannot be defined directly and the notion of "oscillatory modes" defining an IMF is rather confusing. To deal with these problems, multidimensional envelopes are firstly generated by taking a signal's projections along different directions, and then the average of these multidimensional envelopes are taken as the local mean. [9–11]. This calculation of local mean can be considered an approximation of the integral of all envelopes along the multiple projection directions in n-dimensional space; the accuracy of this approximation depends on the uniformity of the chosen direction vectors. Thus, how to choose a suitable set of direction vectors for the projection becomes the main issue. For bivariate signals, points can be uniformly selected along a unit 1-sphere (i.e. a unit circle) where each point represents a direction vector [9]. For trivariate signals, unit quaternion can be used to uniformly select points on a unit 2-sphere [10]. For a general case (n-dimension), quasi-Monte Carlo-based low-discrepancy sequences can be utilized to generate a set of uniformly distributed points on a unit $(n-1)$-sphere [11].

A convenient way of generating a low-discrepancy sequence involves the family of Halton and Hammersley sequences. To generate the Hammersley sequence, let x_1, x_2, …, x_n be the first n prime numbers, then the ith sample of a one-dimensional Halton sequence, denoted by r_i^x, is given by

$$r_i^x = \frac{a_0}{x} + \frac{a_1}{x^2} + \frac{a_2}{x^3} + \ldots + \frac{a_s}{x^{s+1}} \tag{2}$$

where the base-x representation of i is given by

$$i = a_0 + a_1 x + a_2 x^2 + \ldots + a_s x^s \tag{3}$$

Starting from $i=0$, the ith sample of the Halton sequences then becomes

$$(r_i^{x_1}, r_i^{x_2}, \ldots, r_i^{x_n}) \tag{4}$$

The Hammersley sequence is used when the total number of samples, n, is known a priori; in this case, the ith sample within the Hammersley sequence is calculated as

$$(i/n, r_i^{x_1}, r_i^{x_2}, \ldots, r_i^{x_{n-1}}) \tag{5}$$

The Halton and Hammersley sequence-based points correspond to a set of direction vectors, along which projections of an input multivariate signal are calculated. The extrema of such projected signals are interpolated component-wise to yield multidimensional envelopes. The multidimensional envelopes, each of which corresponds to a particular direction vector, are then averaged to obtain the mean of the multivariate signal.

Let $V(t)=[v_1(t), v_2(t), \ldots, v_n(t)]$ be a n-dimensional signal and $X^k = \{x_1^k, x_2^k, \ldots, x_n^k\}$ denote the kth direction vector in a direction set, X. The procedure for multivariate EMD is outlined as follows.

Step 1: Choose a suitable set of direction vectors, X.
Step 2: Calculate the kth projection, $p^k(t)$, of the input signal $V(t)$ along the kth direction vector, X^k, for all k (i.e. $k=1, 2, \ldots, l$ where l is the total number of direction vectors in X).
Step 3: Find the time instants, t_i^k, corresponding to the maxima of the projected signal, $p^k(t)$, for all k.
Step 4: Interpolate $[t_i^k, V(t_i^k)]$ to obtain multivariate envelopes, $E^k(t)$, for all k.
Step 5: The mean is estimated by

$$M(t) = \frac{1}{l}\sum_{k=1}^{l} E^k(t) \tag{6}$$

Step 6: Calculate $D(t)=V(t)-M(t)$. If $D(t)$ fulfills the stopping criterion for a multivariate IMF, then assign $D(t)$ as an IMF and apply the above procedures from Step 2 to $V(t)-D(t)$ to extract the next IMF; otherwise, apply it to $D(t)$.

The stopping criterion for multivariate IMFs is similar to that in standard EMD, the difference being that the condition for equality of the number of extrema and the number of zero crossings is not imposed.

3. Full spectrum analysis

Conventional Fourier spectrum (also called half spectrum) uses real-valued data (i.e. data from one coordinate direction, either X-coordinate or Y-coordinate). In conventional Fourier spectrum, the negative frequency component is the complex conjugate of the positive frequency component. The positive and negative parts of the spectra are mirror images of each other; hence, only the positive half is analyzed. However, individual Fourier spectra conducted on X and Y motions separately are unable to reveal any phase correlation between the X and Y motions. Full spectrum overcomes this limitation by utilizing vibration data from two lateral mutually orthogonal directions together (i.e. X and Y) in the plane of

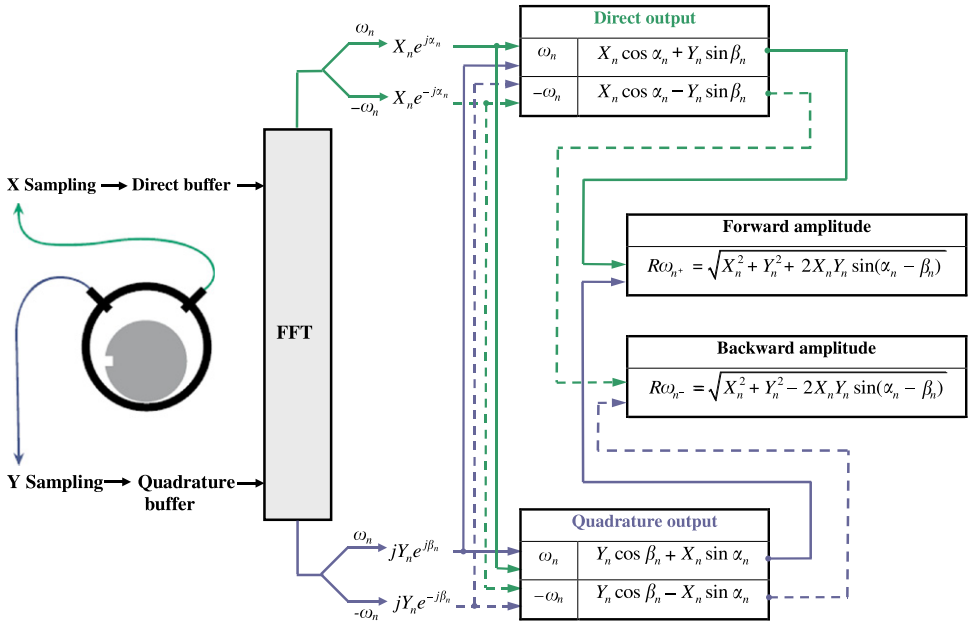

Fig. 1. Procedure of obtaining a full spectrum [13].

rotation. Fig. 1 shows the procedure for obtaining a full spectrum from half spectra of *X* and *Y* signals. Simultaneously sampled *X* signal and *Y* signal are put into the direct and quadrature part of the FFT input, respectively. Consequently, the positive and negative frequency halves of this FFT are not mirror images. Results are then subjected to another transform for *X* to *Y* and for *Y* to *X* precession. In the right half of the full spectrum plot, the amplitudes of the forward whirling frequency components (also known as positive frequency components) are shown. In the left half, the amplitudes of the backward whirling frequency components (also known as negative frequency components) are shown. It is worth noting that an elliptical orbit in one rotating direction is made up of two contra-rotating circular orbits of different amplitudes. The full spectrum considers the rotating directivity, and therefore generates a two-sided spectrum for this elliptical rotation. The full spectrum reveals not only the amplitude but also the directional nature (i.e. either forward or backward) of each frequency component with respect to the rotation direction. There have been a few studies where the researchers have proposed full spectrum-based features for fault diagnosis of rotating machine [14,16,17].

4. A condition monitoring method for rotating machinery

For rotating machinery, full spectrum provides information on both energy (i.e. vibration amplitude) and the directivity of vibration. Depending on the input signal, full spectrum could reveal whether the vibration is in the direction of rotation (i.e. forward) or in the opposite direction of rotation (i.e. backward). When a fault occurs, energy and the directivity of vibration might change. As not all spectral components of the vibration are sensitive to a fault, picking up the most sensitive (fault-affected) spectral component is important.

Fixed band pass filtering can help to pick up spectral components in a certain frequency range; however, prior knowledge of the sensitive frequencies is required before processing the vibration data. Moreover, it is common to have noise contamination in vibration data measurements. If noise is mixed with the frequencies of a true signal, then the fixed band pass filtering process will be ineffective. Empirical mode decomposition can be used as an adaptive filter [19]. An IMF represents a simple oscillatory mode and serves as a filter. Moreover, multivariate EMD, the multivariate extension of EMD, is able to find common oscillatory modes within signals from multiple sources. Thus a complicated rotation represented by two signals (e.g. *x* and *y*) can be decomposed into two sets of IMFs (i.e. IMF_*x* and IMF_*y*) using multivariate EMD. Each IMF in set IMF_*x* (respectively set IMF_*y*) represents a projection of a simpler rotation in the *X* direction (respectively *Y* direction). That is a complicated rotation is decomposed into a set of simple rotations. In this way, selection of the most sensitive spectral component (i.e. a simple rotation) can be achieved by selecting the most sensitive IMF.

To select the sensitive IMF, criteria based on the correlation coefficient between an IMF and its raw signal was used in [4,20,21]. Note that the correlation coefficient reflects only linear relationships. To account for nonlinear relationships as well, mutual information [22] is employed here. A criterion is proposed that takes into account two kinds of mutual information: that between the *n*th IMF and its raw signal, and that between the *n*th IMF of a signal with certain health condition and the *n*th IMFs of signals with different health conditions.

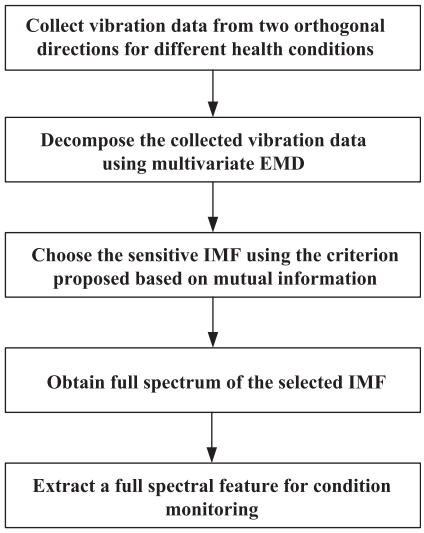

Fig. 2. Flow chart of the proposed method.

Suppose that two signals, $x_{nor}(t)$ and $y_{nor}(t)$, collected from the X and Y directions under the normal operation, are denoted by a two-dimensional signal, $x_{nor}(t)\vec{i}+y_{nor}(t)\vec{j}$; two signals, $x(t)$ and $y(t)$, collected from the X and Y directions at a fault condition, are denoted by a two-dimensional signal, $x(t)\vec{i}+y(t)\vec{j}$. Let $cn_{xnor}(t)$, $cn_{ynor}(t)$, $cn_x(t)$, and $cn_y(t)$ be the nth IMF of $x_{nor}(t)$, $y_{nor}(t)$, $x(t)$ and $y(t)$, respectively, obtained by multivariate EMD. The proposed criterion for selecting a sensitive IMF is described below.

(1) Calculate the mutual information, a_n, between the nth IMF of a two-dimensional normal signal, $cn_{xnor}(t)\vec{i}+cn_{ynor}(t)\vec{j}$, and its raw signal, $x_{nor}(t)\vec{i}+y_{nor}(t)\vec{j}$.
(2) Calculate the mutual information, b_n, between the nth IMF of a two-dimensional fault signal, $cn_x(t)\vec{i}+cn_y(t)\vec{j}$, and its raw signal, $x(t)\vec{i}+y(t)\vec{j}$.
(3) Calculate the mutual information, e_n, between $cn_{xnor}(t)\vec{i}+cn_{ynor}(t)\vec{j}$ and $cn_x(t)\vec{i}+cn_y(t)\vec{j}$.
(4) Calculate the sensitivity factor, λ_n, for the nth IMF using

$$\lambda_n=\frac{a_n+b_n}{2}-e_n \tag{7}$$

In Eq. (7), the first part, $(a_n+b_n)/2$, represents the average mutual information between the nth IMFs and their raw signals; the second part, e_n, represents the mutual information between the nth IMF of the normal signal and the nth IMF of the signal under different health conditions (i.e. the fault signal in this example). To ensure that an IMF is informative enough to represent the original signal, the first part of Eq. (7) is supposed to be high; to enable the easy detection of the fault, and the second part is supposed to be low. The higher the λ_n value, the more sensitive the IMF.

After the sensitive IMF is selected, full spectrum of this IMF is obtained and then a proper full spectral feature is extracted for condition monitoring. A flow chart of the proposed method is given in Fig. 2.

5. Experiment results

5.1. Simulation experiment

In the fault diagnosis of rotating machinery, a change of the amplitude at a typical frequency [23] and the appearance of a new frequency [24] are two phenomena that commonly occur when a fault occurs. For this reason, simulation signals were constructed considering these two effects to illustrate and test the proposed method.

For simplicity, four signals, namely x_0, y_0, x_1 and y_1, are constructed and their mathematical expressions are stated as Eqs. (8)–(11). The x_0, y_0 and x_1, y_1 are two sets of orthogonal vibration signals measured from the X and Y directions for "normal" and "fault" conditions respectively. Vibration signals for normal condition have of two parts: the first part is an anti-clockwise rotation at a frequency of 20 Hz with amplitude of 0.5; the second part is an anti-clockwise rotation at 100 Hz with amplitude of 1. Vibration signals for the fault condition consist of four parts: the first part is the same as the first part of the normal signals; the second part is an anti-clockwise rotation at 50 Hz with amplitude of 0.2; the third part

is a clockwise rotation at 50 Hz with amplitude of 1; the fourth part is the same as the second part of the normal signals but with amplitude of 0.9.

$$x_0 = 0.5\cos(40\pi t)+\cos(200\pi t) \tag{8}$$

$$y_0 = 0.5\sin(40\pi t)+\sin(200\pi t) \tag{9}$$

$$x_1 = 0.5\cos(40\pi t)+0.2\cos(100\pi t)+\cos(-100\pi t)+0.9\cos(200\pi t) \tag{10}$$

$$y_1 = 0.5\sin(40\pi t)+0.2\sin(100\pi t)+\sin(-100\pi t)+0.9\sin(200\pi t) \tag{11}$$

First, standard EMD is applied to x_0, y_0, x_1 and y_1, separately; the results are shown in Fig. 3. The top row in each column shows the raw signals, the bottom row shows the residuals, and the middle rows are IMFs. There are two IMFs for x_0 and y_0, while three for x_1 and y_1. Thus standard EMD results in an unequal number of IMFs [8], making it impossible to compare normal and fault signals on the 3rd IMF. Moreover, the frequency content of the 2nd IMFs of x_0 and y_0 (i.e. 20 Hz) is different from that of the 2nd IMFs of x_1 and y_1 (i.e. 50 Hz), therefore, the 2nd IMFs of the normal and fault signals cannot be compared either. From this simple simulation example, it can be seen that it would be difficult to capture fault information from the same IMF number for real vibration signals, because real vibration signals are much more complicated than those considered in Eqs. (10) and (11).

As stated in Section 2, multivariate versions of EMD are proposed to ensure proper decomposition of signals from different sources. In this example, for each health condition, two signals are measured at two orthogonal directions. If bivariate EMD is applied to normal signals (i.e. $x_0\vec{i}+y_0\vec{j}$) and fault signals (i.e. $x_1\vec{i}+y_1\vec{j}$) separately, the results will be the same as those shown in Fig. 3. The problem of unmatched decomposition in number and property still exists. The problem of unmatched decomposition could be avoided by decomposing all the signals together. First, all the four raw signals (i.e. x_0, y_0, x_1, and y_1) are combined to form a four-dimensional signal, $x_0\vec{i}+y_0\vec{j}+x_1\vec{k}+y_1\vec{q}$. Multivariate EMD is then conducted to decompose the four-dimensional signal. A set of four-dimensional IMFs, $cn_{x0}\vec{i}+cn_{y0}\vec{j}+cn_{x1}\vec{k}+cn_{y1}\vec{q}$, are obtained, where cn_{x0}, cn_{y0}, cn_{x1}, and cn_{y1} represent the nth IMF of x_0, y_0, x_1, and y_1, respectively. Results are shown in Fig. 4. The top row shows the raw signals. The bottom row shows the residuals. The 1st, 2nd and 3rd IMFs are

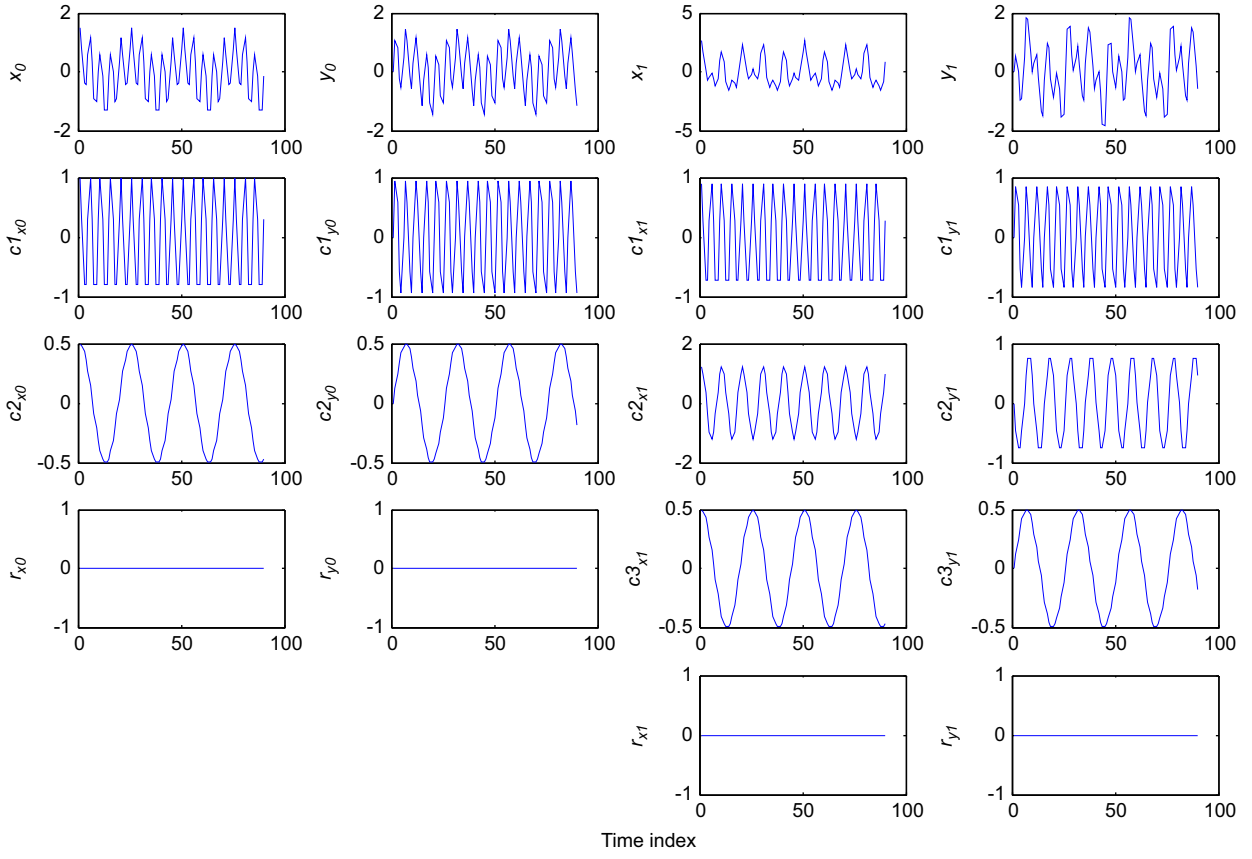

Fig. 3. Decomposition results of simulated data with standard EMD.

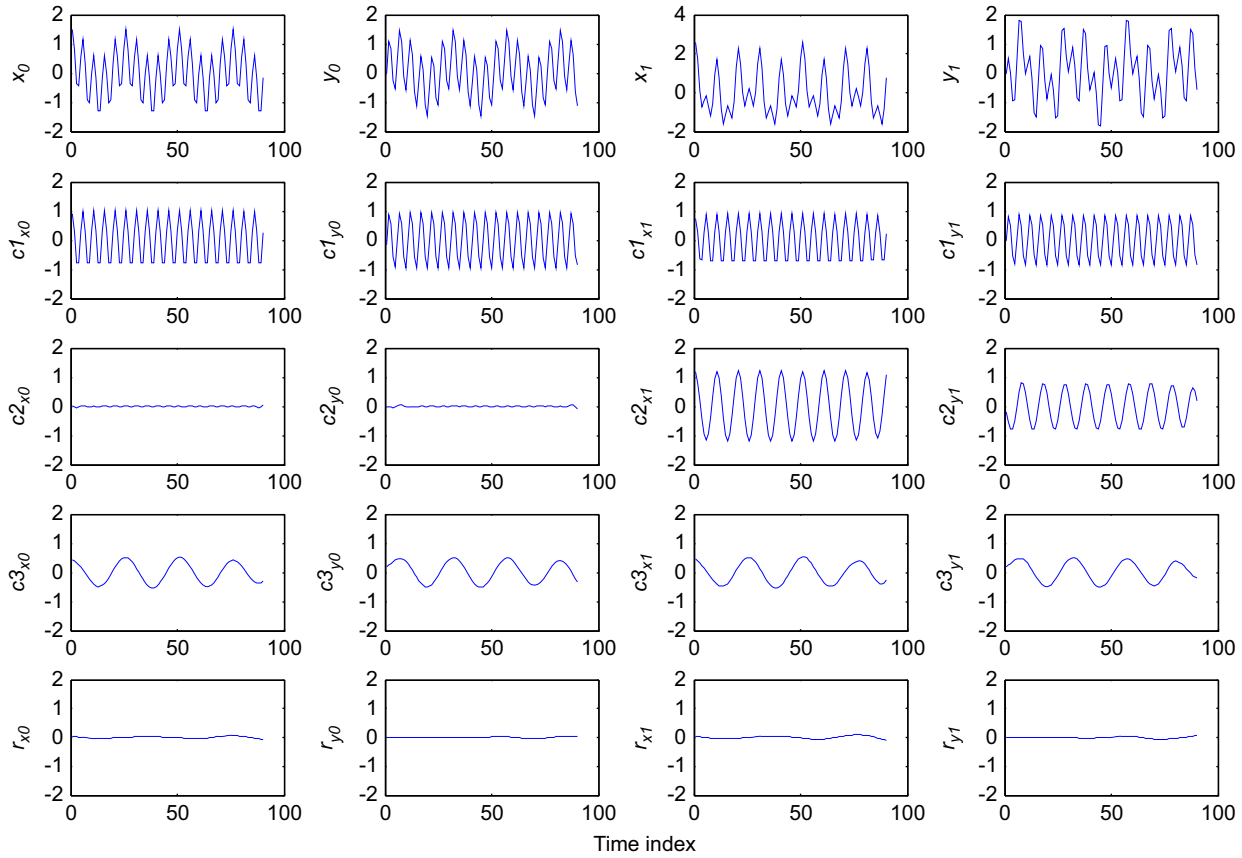

Fig. 4. Decomposition results of simulated data with multivariate EMD.

Table 1
Sensitivity factor of each IMF (simulated data).

IMF #	Sensitivity factor
1	−1.53
2	**0.51**
3	−2.51

shown in the second, third and fourth row for frequencies 100, 50 and 20 Hz, respectively. The 2nd IMFs of x_0 and y_0 have no element for 50 Hz; therefore their 2nd IMFs are almost 0. Now each row has a common frequency content, which makes the IMFs of normal and fault signals comparable. It can also be seen that the raw complicated motion are decomposed into three simple rotations, making further inference regarding the fault sensitive IMF easier.

The sensitivity factor based on mutual information is then calculated to find a sensitive IMF which can clearly distinguish the fault condition. Table 1 shows the details. The 2nd IMF gives the highest value and therefore is chosen as the sensitive IMF. This result is consistent with our intuition because the 2nd IMF, as can be seen from Fig. 4, shows a clear difference between normal and fault signals.

To express the fault information, full spectrum is conducted on the sensitive IMF (i.e. the 2nd IMF). The 2nd IMFs of x_m and y_m (where $m=\{0, 1\}$) are used as direct part and quadrature part, respectively. The full spectra of $c2_{x0}\vec{i}+c2_{y0}\vec{j}$ (normal) and $c2_{x1}\vec{i}+c2_{y1}\vec{j}$ (fault) are shown on the top of Fig. 5. To facilitate comparison, the half spectra are also shown in the middle row ($c2_{x0}$ and $c2_{x1}$) and the bottom row ($c2_{y0}$ and $c2_{y1}$). The 2nd IMFs of normal signals are almost zero, so the spectra in the three rows are almost zero for the normal case. The characteristic of full spectrum can be observed by checking the fault case. Full spectrum clearly indicates the backward (i.e. clockwise) rotation with amplitude of 1 and the forward (i.e. anti-clockwise) rotation with amplitude of 0.2, as defined in Eqs. (10) and (11). The half spectra does not, however, take rotation directivity into account, therefore, the term $c2_{x1}$, $0.2\cos(100\pi t)+\cos(-100\pi t)$, is regarded simply as $1.2\cos(100\pi t)$ and the amplitude of 1.2 is equally split to the amplitudes at 50 and -50 Hz (i.e. 0.6). The same reasoning

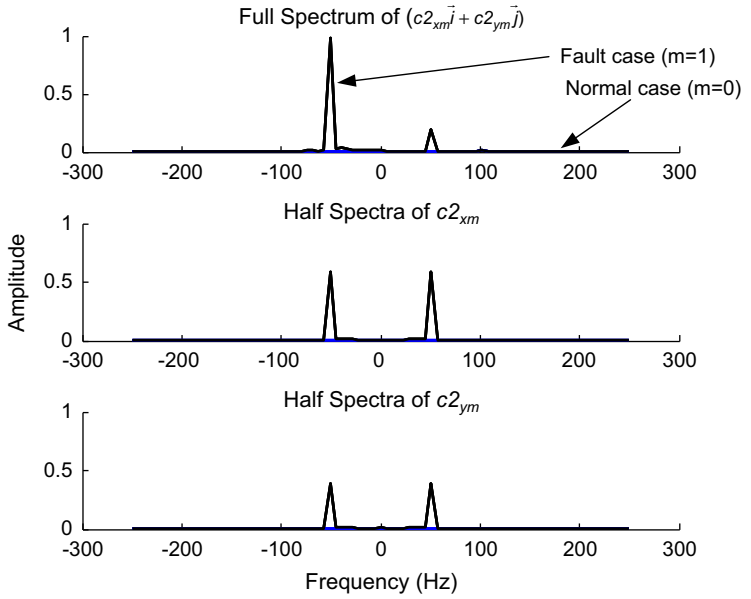

Fig. 5. Full spectra and half spectra of the 2nd IMFs of simulated data.

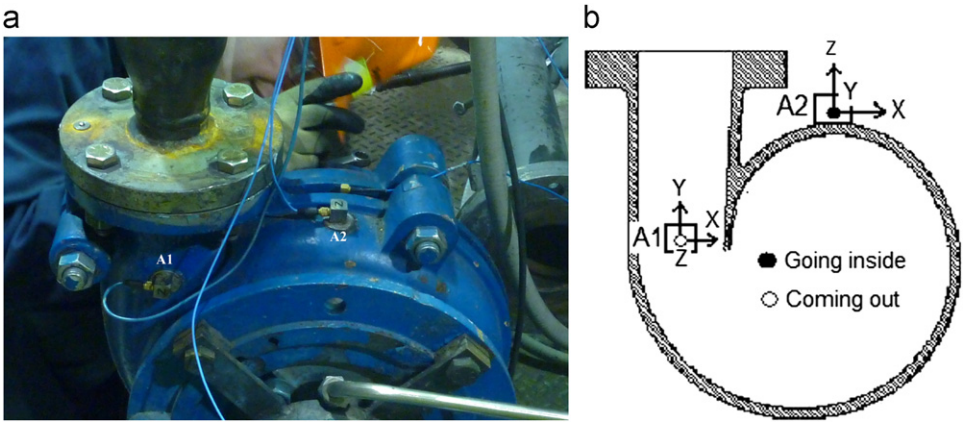

Fig. 6. (a) Vibration sensor locations with labels; (b) Schematic for direction convention.

applies to $c2_{y1}$, $0.2\sin(100\pi t)+\sin(-100\pi t)$, at -50 and 50 Hz both amplitudes are 0.4. Compared to the half spectra which gives amplitudes of 0.6 for $c2_{x1}$ and 0.4 for $c2_{y1}$, the full spectrum with amplitude of 1 at -50 Hz and amplitude of 0.2 at 50 Hz reveals the fault information more clearly with regard to both directivity and energy.

5.2. Impeller vane trailing edge damage experiment

Centrifugal pumps are widely used for moving slurries in many applications, such as the oil sands and mining. Pumping slurries causes severe wear of the wetted components, e.g. impellers. Khalid and Sapuan [25] noted that the vane trailing edge of an impeller encounters more wear compared to the vane leading edge. In this work, we focus on the wear at the vane trailing edge. Most of the past studies on wear caused by pumping slurries focused on finding relationships between wear and various operation and/or design parameters. The effects of impeller wear on vibration have been studied little. Mani et al. [26] suggested using a cumulative amplitude measure for detecting impeller wear. Zhao et al. [27] studied the detection of initial impeller wear using rough set. In this section, the proposed method is applied to monitor the condition of an impeller vane trailing edge.

To track damage development at the vane trailing edge, four damage levels are considered: no damage (level 0), slight damage (level 1), medium damage (level 2) and severe damage (level 3). Each of the five vanes of an impeller was shortened by 0%, 22%, 26% and 29.3% in length, respectively. For each damage level, vibration data were collected at a sampling frequency of 5 KHz in lab experiments with the pump running at 2400 RPM at the best efficient point (BEP). The vibration sensors employed are labeled in Fig. 6.

In pumps, hydrodynamic forces are often the major sources of vibration [28]. The velocity distribution at the impeller outlet is non-uniform as a result of the finite vane thickness, the blockage caused by the boundary layers, and possible flow separation. The cutwater is thus approached by an unsteady flow inducing alternating hydrodynamic forces on the cutwater. These hydrodynamic forces cause the vibrations of the pump casing. It is believed that the changes of impeller geometry change the velocity and the pressure distributions inside the pump. Consequently the hydrodynamic forces and therefore the vibrations are affected. To better understand possible changes in the flow field, numerical simulations were carried out using the computational fluid dynamics (CFD) approach. Fig. 7 shows the relative velocity fields near the cutwater under the four health conditions. The direction of impeller rotation is clockwise. The flow goes out from the impeller into the volute, experiences a 360 degree rotation in the volute, and comes out to the outlet. Thus near the cutwater area, part of the flow is directed into the volute (forward direction), and the rest is directed to the outlet (backward direction). For the no damage case (Fig. 7(a)), the velocity vectors are well directed towards the outlet and volute. The velocity vectors are clearly in the direction of rotation. This directivity is distorted when damage occurs at the vane trailing edge. The degree of distortion increases as the level of damage increases. At the severe case, the flow has an obviously weak trend in the forward direction.

The vibration sensor labeled A1 (Fig. 6) is expected to capture the change of flow directivity indicated in Fig. 7, because it is located close to the cutwater. Data from the X and Y directions of sensor A1 are analyzed in this paper. Based on the flow patterns shown in Fig. 7, the forward whirling becomes weak compared to the backward whirling, so we can expect the ratio between the backward whirling energy and the forward whirling energy to increase as the damage level increases. A full spectral feature in the form of an energy ratio is defined using Eq. (12) to represent this. In Eq. (12), $a(f)$ represents the value of amplitude at frequency f in a full spectrum.

Let x_0, x_1, x_2, and x_3 (respectively y_0, y_1, y_2, and y_3) denote the signal measured by A1-X (respectively A1-Y) for the no damage, slight damage, medium damage and severe damage cases, respectively. Fig. 7 shows that the impeller rotates clockwise. To ensure the forward direction is the impeller's rotation direction, signals from A1-X and A1-Y are used as the quadrature part and direct part in the calculation of full spectrum, respectively. Full spectra of the raw data are shown in Fig. 8 for each health condition and the change in energy ratio with the damage level is shown in Fig. 9. It can be seen that the spectra consist of many spectral components. Though the spectra are different for different health conditions, there is no monotonic trend observed. Empirical mode decomposition which is capable of filtering spectral components is thus needed.

$$Er = \frac{\sqrt{\sum_{f<0} a(f)^2}}{\sqrt{\sum_{f>0} a(f)^2}} \tag{12}$$

Although standard EMD could generate the same number (ten in this experiment) of IMFs for signals from different sources, there still remains an unmatched property problem. Fig. 10 shows the 4th IMF as an example. The frequency

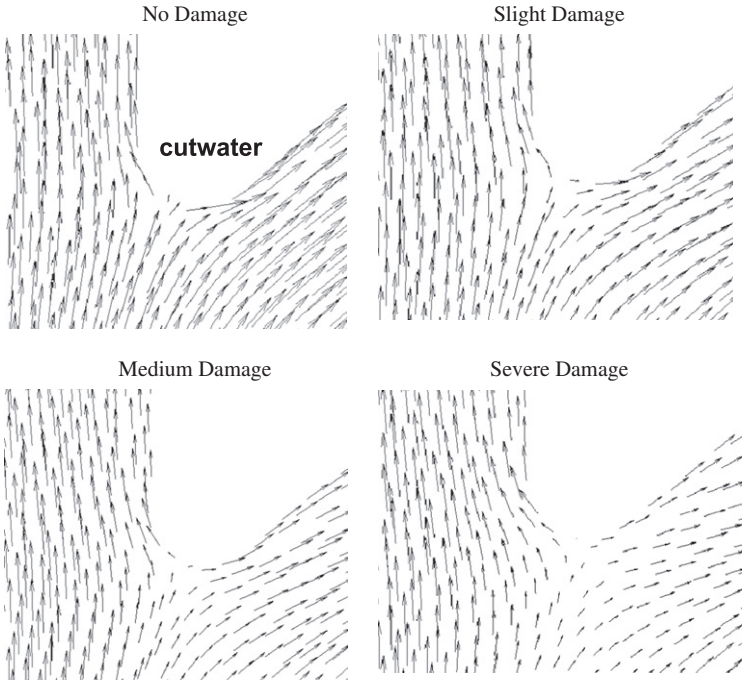

Fig. 7. Zoomed view of the relative velocity fields near the cutwater area.

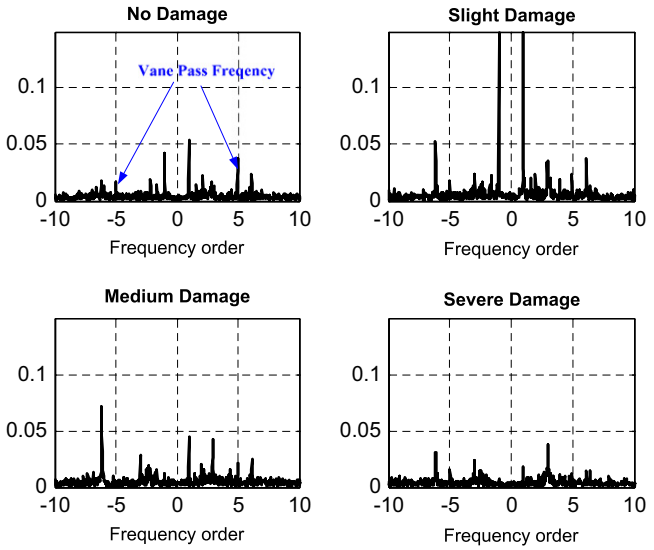

Fig. 8. Full spectra of raw data for different health conditions.

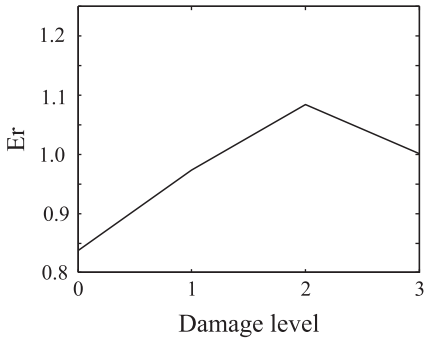

Fig. 9. Change in energy ratio of raw signal with damage level.

contents of the 4th IMFs for different damage levels don't match. The frequency centers of the 4th IMFs for x_0, x_1, and x_2 signals are around 1.5*X* (i.e. 1.5 times the pump rotation frequency); however, the frequency center of the 4th IMF of x_3 signal is around 2*X*. This inconsistency also exists for signals measured by A1-Y. At the same damage level, the 4th IMFs of signals measured in different directions don't match either. For example, in the no damage case, the frequency center of the 4th IMF of x_0 signal is 1.5*X*, whereas the frequency center of the 4th IMF of y_0 signal is 1*X*. There is inconsistency in the slight and medium damage cases too. To solve the unmatched property of IMFs from different sources, multivariate EMD should be applied.

Eight raw signals (i.e. x_0, y_0, x_1, y_1, x_2, y_2, x_3 and y_3) are combined into an eight-dimensional signal and decomposed together by multivariate EMD algorithm. Fig. 11 shows the decomposition results for y_0 and y_3 signals (the results for data associated with other health conditions are not presented here). The first ten IMFs are obtained for each signal; the other IMFs have small amplitudes and thus are put into the residual (r). It can be seen that the corresponding IMFs of y_0 and y_3 signals carry the same frequency content. The criterion proposed in Section 4 is used to evaluate the significance of each of the ten IMFs. The significance factor of the nth IMF is calculated using the averaged mutual information between the nth IMF and its raw signal subtracted by the averaged mutual information between the nth IMF of one health condition and that of other health conditions. Table 2 shows the results. The 4th IMF has the highest value and is chosen as the sensitive IMF.

The 4th IMF of x_i signal and the 4th IMF of y_i signal are used to obtain the full spectrum for each of the four health states (Fig. 12). At the no damage condition, the forward whirling frequencies are dominant. As the health condition worsens, the strength of the forward whirling components compares unfavorably with that of the backward whirling components. This is further examined by plotting the energy ratio (Eq. (12)) values in Fig. 13. It can be seen that the ratio between backward whirling components and forward whirling components monotonically increases as the damage level increases. This agrees with the observation from Fig. 7. Furthermore, as described at the beginning of Section 5.2, the local flow field near

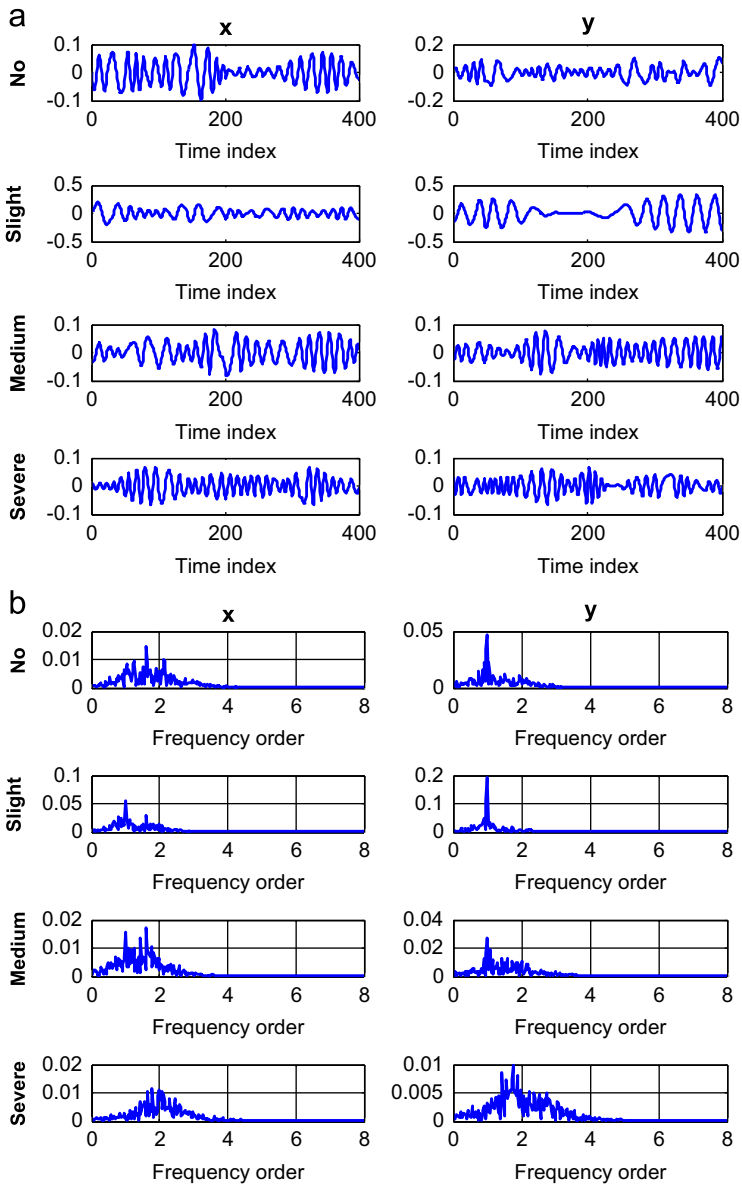

Fig. 10. (a) 4th IMF of different signals in the time domain (standard EMD). (b) 4th IMF of different signals in the frequency domain (standard EMD).

cutwater is subjected to significant variations each time an impeller vane passes it, so the vane passing frequency should be the characteristic frequency. Fig. 12 shows that the selected IMF is centered around the vane passing frequency; this is consistent with our expectation.

5.3. *Rotor-stator rub experiment*

Contact between the rotating element and the stationary element is a serious malfunction in the rotating machinery which could result in a catastrophic failure of the machine [29]. There have been different physical phenomena such as impacting, friction, and stiffening involved in the rotor-stator interactions, all of which additionally affected by thermal effects. Depending upon the operating conditions and the physical configuration of the rotor-stator, one or more of these physical phenomena prevails and governs the vibration response. It has been established that rotor-stator rub is a nonlinear and often non-stationary malfunction, which exhibits a variety of nonlinear response characteristics such as periodic, quasi-periodic and chaotic vibrations [24,29].

Researchers have investigated rotor motion for a variety of the rubbing conditions. Groll and Ewins [30] found subharmonic and superharmonic frequencies in steady state vibration response due to rotor-stator interactions. Strong subharmonic measured was sometimes as low as $X/32$, and strong superharmonic measured was sometimes as high as $9X$.

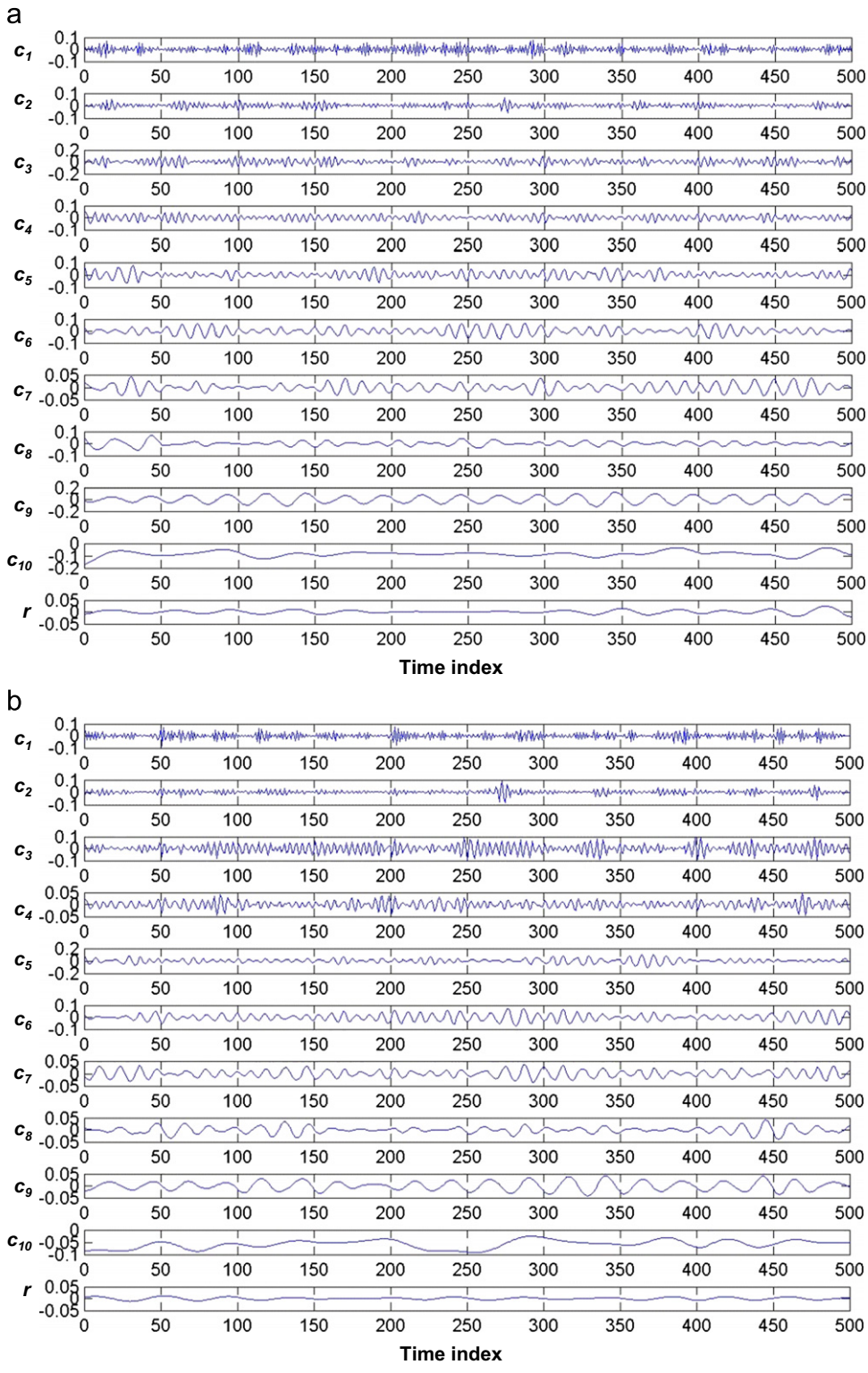

Fig. 11. Decomposition results for y_0 (a) and y_3(b) using multivariate EMD.

Patel and Darpe [17] discussed the use of spectrum cascade for identification of rub and showed the existence of pseudo-resonance and backward whirling components. Li and Paidoussis [31] showed that the vibration motion can be forward or backward whirling, depending upon the parameters. Ma et al. [32] identified rotor trajectory and time and frequency

Table 2
Sensitivity factor of each IMF (impeller data).

IMF #	Sensitivity factor
1	0.09
2	0.16
3	0.19
4	**0.24**
5	0.12
6	0.21
7	0.05
8	−0.11
9	−0.35
10	−0.77

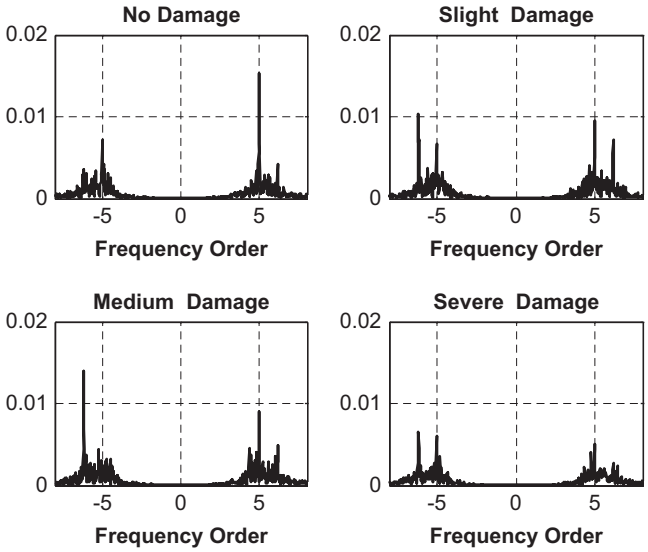

Fig. 12. Full spectra of the 4th IMF of different signals (multivariate EMD).

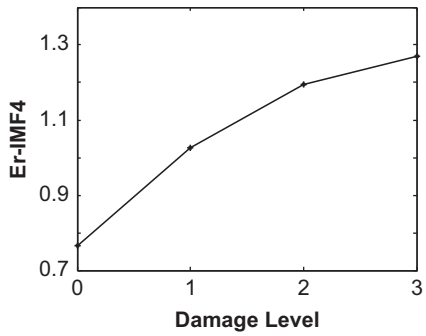

Fig. 13. Trend of energy ratio of the 4th IMF with damage level (multivariate EMD).

features for the bearing rub impacts in a rotor system. For a slight rub, the rotor trajectory remains forward whirling, whereas for a severe rub it becomes backward whirling. All previous studies compared results from vibration signals at no-rub and with-rub conditions and focused on the presence/absence of some of the spectral and/or time-frequency features. None of the studies presented a conclusive frame work for rotor-stator rub detection. In this study the proposed algorithm provides such an approach for the rotor-stator rub diagnosis. The idea is to extract the whirling character of the vibration motion in some frequency bands through the use of multivariate EMD and mutual information theory.

Experiments were carried out on a rotor bearing system that consists of a circular steel shaft with a central disk supported on a pair of ball bearings (Fig. 14). The central disk weighs 5.65 kg. The shaft is 25 mm in diameter and its bearings are 0.7 m apart. Single row deep groove ball bearings (SKF 6204) were used to support the rotor. A Siemens 750 W 3-phase induction motor with Micromaster controller drove the system through three jaw flexible couplings. Motor shaft and rotor shaft were aligned using the reverse dial indicator method. Provision was made to induce rub on the disk. Through the use of a rub bolt ($M30 \times 1.5$), which could move along the vertical direction, the desired amount of rub can be induced. Initial gap between the rub bolt and the disk was kept at 0.25 mm. So, there would be no contact between the rub screw and the disk. The rub screw was then rotated by a one-third turn, two-third turn and one-full turn thus moving the screw upward from the initial position by 0.5, 1.0 and 1.5 mm, respectively. Each time, the locknut was tightened to further restrict movement of the bolt. For each of these bolt movements, the rub between disk and bolt can be termed slight rub, medium rub and severe rub, respectively.

Vibrations were sensed using Bently Nevada eddy current proximity probes (3300 series). A stopper was provided above the disk, to limit vibration levels to avoid damage to the vibration sensors. Two probes were used to monitor vibrations in the horizontal and vertical directions. One additional probe was kept near the coupling, the signal from which acted as the reference signal. Vibrations sensed by the probes were conditioned by Proximeter® before being sent to an A/D card plugged into the computer. A Labview™ program was written to acquire the vibration data using an A/D card.

Experiments were carried out at different damage levels: no-rub (level 0), slight rub (level 1), medium rub (level 2) and severe rub (level 3). In each experiment, a rotor shaft was rotated at 24 Hz and the steady state lateral vibration signals were recorded using probes in horizontal and vertical directions. The acquired signals were stored and processed further to investigate the effectiveness of the proposed diagnostic approach.

As reported by Ma et al. [32], compared to the forward whirling spectral components, increase in the amplitude of the backward whirling spectral component is expected to be more as a result of the rub fault. So, we calculated the energy ratio defined in Eq. (12) from vibration signals acquired under different rub conditions. It can be seen from Fig. 15 that there is no monotonic trend in it. This is due to the fact that only some of the spectral components generated by a rub fault are backward whirling; there are others that are forward whirling.

Next, the proposed approach is applied. Vibration signals acquired from no rub (x_0, y_0), slight rub (x_1, y_1), medium rub (x_2, y_2) and severe rub (x_3, y_3) conditions are considered together and a total of nine IMFs are extracted using multivariate EMD. As explained in Section 2 and demonstrated in Sections 5.1 and 5.2, irrespective of the frequency content, the same number of IMFs are extracted from each signal. Fig. 16 shows the IMFs extracted from y_0 and y_3 signals. The significance factor for each of the nine IMFs has been calculated using the averaged mutual information between raw signals and its

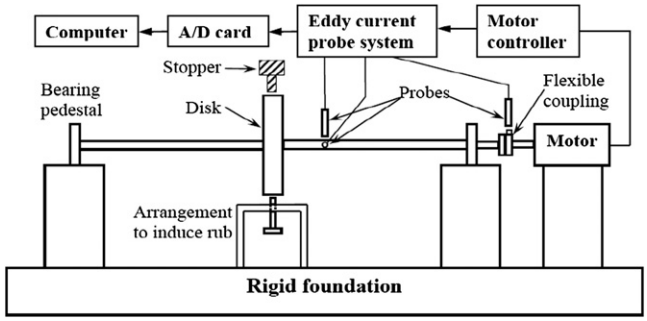

Fig. 14. Schematic of a rotor-stator rub experiment set-up.

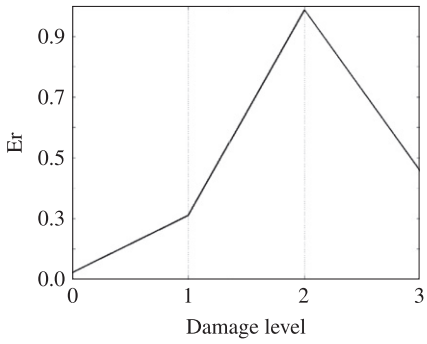

Fig. 15. Change in energy ratio of raw signal with rub severity.

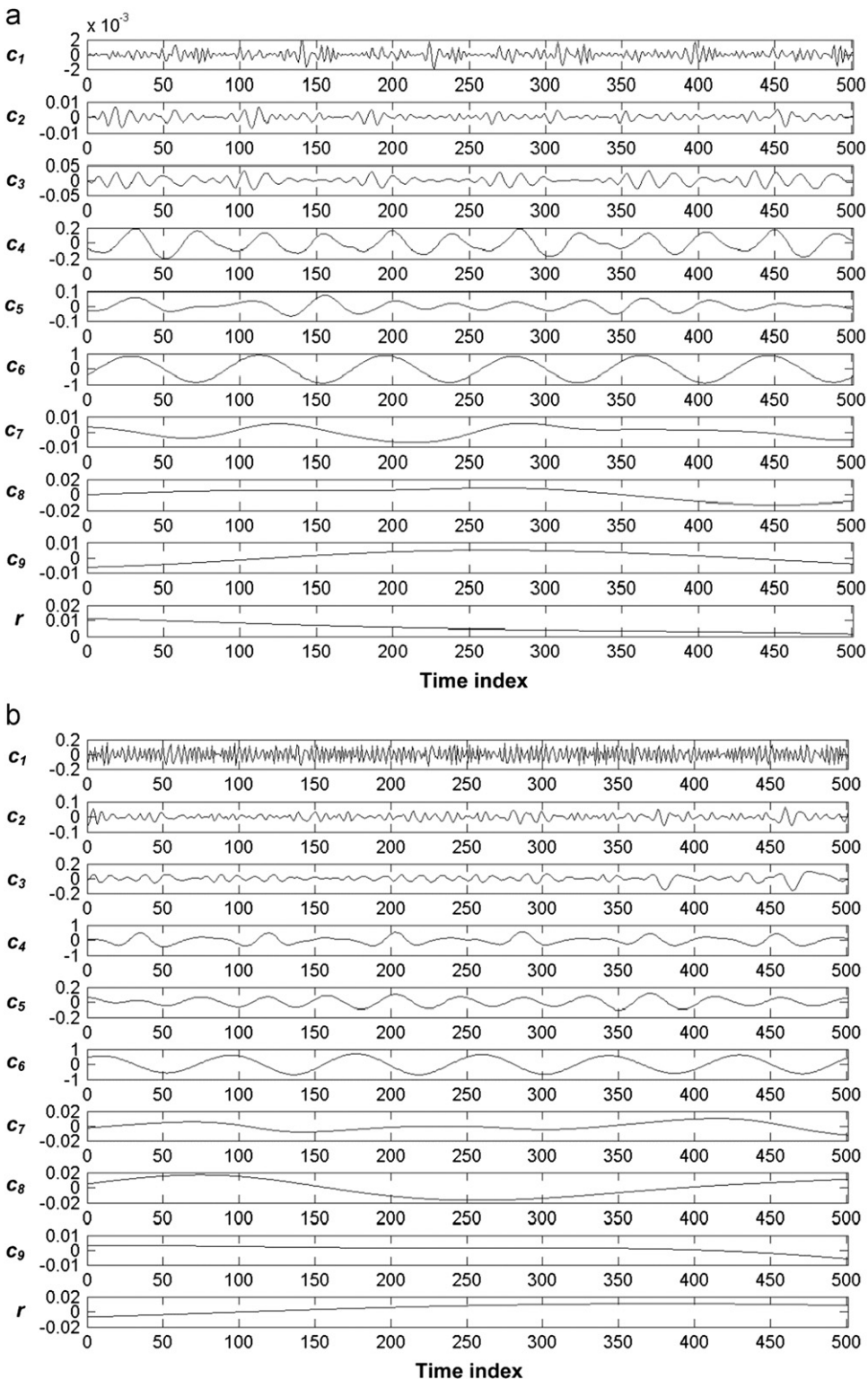

Fig. 16. Decomposition results for y_0 (a) and y_3 (b) using multivariate EMD.

IMF subtracted by the averaged mutual information between the IMF in one health condition and that in other health conditions. Table 3 shows the results for each IMF. The 4th IMF has the highest positive value and thus is chosen as the sensitive IMF.

Table 3
Sensitivity factor of each IMF (rotor-stator data).

IMF #	Sensitivity factor
1	0.30
2	0.36
3	0.82
4	**0.99**
5	−1.18
6	−0.52
7	−3.29
8	−3.71
9	−3.93

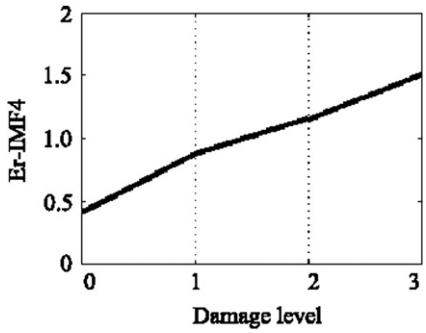

Fig. 17. Trend of energy ratio of the 4th IMF with rub severity (multivariate EMD).

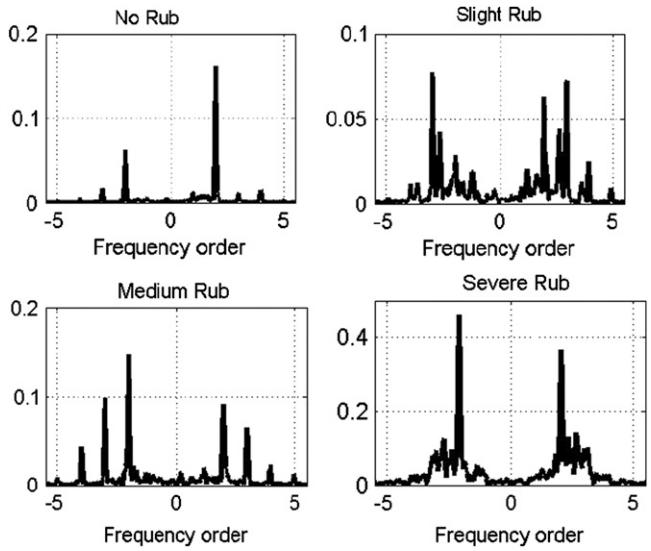

Fig. 18. Full spectra of the 4th IMF for different health conditions (multivariate EMD).

The full spectra are obtained for the 4th IMF of (x_0, y_0), (x_1, y_1), (x_2, y_2) and (x_3, y_3) signals. Fig. 17 shows the trend of the energy ratio between the backward whirling component and the forward whirling components as the damage level increases. It can be seen that it has a clear increasing monotonic trend. On examining each individual full spectrum for no-rub, slight rub, medium rub and severe rub for the 4th IMF (Fig. 18), it can be seen that the frequency contained in this IMF gains strength in backward direction as rub severity increases.

6. Conclusions

This paper proposed a method to extract a feature from multiple sensors for the condition monitoring of rotating machinery based on multivariate EMD and full spectrum. Multivariate EMD is employed to decompose signals from

different sources (either different sensors or different health conditions) together, thus a complicated rotation can be represented by a set of simpler rotation components. Multivariate EMD is proved to outperform standard EMD for multivariate signals, because it is able to ensure that IMFs from different sources do not differ in number or frequency content. Thus the comparison of IMFs for different health conditions is made reasonable and easy. A criterion based on mutual information is proposed for selecting the most sensitive IMF. This criterion is defined to give credit to the IMF which better represents the raw signal and to penalize the IMF which is less able to distinguish different health conditions. Thus, the selected IMF always ensures that it retains the unique information of a certain health condition. For monitoring damage in an impeller and rub faults in a rotor-stator, a full spectral feature is established in the form of the ratio between the energy of backward whirling components and the energy of forward whirling components; the physical explanations of this feature are verified using numerical simulations of the flow fields in the pump and a review of literatures on rotor-stator rub, respectively. Although the usefulness of the proposed method is shown using only one full spectral feature, the approach presented is general and can be extended for more full spectral features.

Acknowledgment

This research was supported by Syncrude Canada Ltd. and the Natural Sciences and Engineering Research Council of Canada (NSERC). The authors would like to acknowledge the valuable suggestions provided by Professor Carlos Lange on our CFD simulation. Comments from reviewers are very much appreciated.

References

[1] Z. Ge, U. Kruger, L. Lamont, L. Xie, Z. Song, Fault detection in non-Gaussian vibration systems using dynamic statistical-based approaches, Mechanical Systems and Signal Processing 24 (2010) 2972–2984.
[2] J. Lin, L. Qu, Feature extraction based on morlet wavelet and its application for mechanical fault diagnosis, Journal of Sound and Vibration 234 (2000) 135–148.
[3] Y. Lei, Z. He, Y. Zi, Q. Hu, Fault diagnosis of rotating machinery based on multiple ANFIS combination with GAs, Mechanical Systems and Signal Processing 21 (2007) 2280–2294.
[4] Z.K. Peng, P.W. Tse, F.L. Chu, An improved Hilbert-Huang transform and its application in vibration signal analysis, Journal of Sound and Vibration 286 (2005) 187–205.
[5] B. Liu, S. Riemenschneider, Y. Xu, Gearbox fault diagnosis using empirical mode decomposition and Hilbert spectrum, Mechanical Systems and Signal Processing 20 (2006) 718–734.
[6] Y. Yang, D.J. Yu, J.S. Cheng, A fault diagnosis approach for roller bearing based on IMF envelope spectrum and SVM, Measurement 40 (2007) 943–950.
[7] N.E. Huang, Z. Shen, S.R. Long, M.L.C. Wu, H.H. Shih, Q.N. Zheng, N.C. Yen, C.C. Tung, H.H. Liu, The empirical mode decomposition and the Hilbert spectrum for nonlinear and non-stationary time series analysis, Proceedings of the Royal Society of London Series A—Mathematical Physical and Engineering Sciences 454 (1998) 903–995.
[8] D. Looney, D.P. Mandic, Multiscale image fusion using complex extensions of EMD, IEEE Transactions on Signal Processing 57 (2009) 1626–1630.
[9] G. Rilling, P. Flandrin, P. Goncalves, J.M. Lilly, Bivariate empirical mode decomposition, IEEE Signal Processing Letters 14 (2007) 936–939.
[10] N. Rehman, D.P. Mandic, Empirical mode decomposition for trivariate signals, IEEE Transactions on Signal Processing 58 (2010) 1059–1068.
[11] N. Rehman, D.P. Mandic, Multivariate empirical mode decomposition, Proceedings of the Royal Society A: Mathematical, Physical and Engineering Science 466 (2010) 1291–1302.
[12] I. Tsoumas, G. Georgoulas, A. Safacas, G. Vachtsevanos, Empirical mode decomposition of the stator start-up current for rotor fault diagnosis in asynchronous machines, in: Proceedings of the 2008 International Conference on Electrical Machines, Vilamoura, Portugal 2008, pp. 1–6.
[13] P. Goldman, A. Muszynska, Application of full spectrum to rotating machinery diagnostics, Orbit, First Quarter (1999) 17–21.
[14] C.W. Lee, Y.S. Han, The directional Wigner distribution and its applications, Journal of Sound and Vibration 216 (1998) 585–600.
[15] N. Baydar, Q. Chen, A. Ball, U. Kruger, Detection of incipient tooth defect in helical gears using multivariate statistics, Mechanical Systems and Signal Processing 15 (2001) 303–321.
[16] F.Q. Wu, G. Meng, Compound rub malfunctions feature extraction based on full-spectrum cascade analysis and SVM, Mechanical Systems and Signal Processing 20 (2006) 2007–2021.
[17] T.H. Patel, A.K. Darpe, Use of full spectrum cascade for rotor rub identification, Advances in Vibration Engineering 8 (2009) 139–151.
[18] N.E. Huang, M.-L.C. Wu, S.R. Long, S.S.P. Shen, W. Qu, P. Gloersen, K.L. Fan, A confidence limit for the empirical mode decomposition and Hilbert spectral analysis, Proceedings of the Royal Society of London. Series A: Mathematical, Physical and Engineering Sciences 459 (2003) 2317–2345.
[19] P. Flandrin, G. Rilling, P. Goncalves, Empirical mode decomposition as a filter bank, IEEE Signal Processing Letters 11 (2004) 112–114.
[20] C.C. Lin, P.L. Liu, P.L. Yeh, Application of empirical mode decomposition in the impact-echo test, NDT and E International 42 (2009) 589–598.
[21] Y.G. Lei, M.J. Zuo, Fault diagnosis of rotating machinery using an improved HHT based on EEMD and sensitive IMFs, Measurement Science & Technology 20 (2009) 1–12.
[22] A. Kraskov, H. Stogbauer, P. Grassberger, Estimating mutual information, Physical Review E 69 (2004) 1–16.
[23] X. Fan, M.J. Zuo, Gearbox fault detection using Hilbert and wavelet packet transform, Mechanical Systems and Signal Processing 20 (2006) 966–982.
[24] F. Chu, W. Lu, Experimental observation of nonlinear vibrations in a rub-impact rotor system, Journal of Sound and Vibration 283 (2005) 621–643.
[25] Y.A. Khalid, S.M. Sapuan, Wear analysis of centrifugal slurry pump impellers, Industrial Lubrication and Tribology 59 (2007) 18–28.
[26] G. Mani, D. Wolfe, X. Zhao, M.J. Zuo, Slurry pump wear assessment through vibration monitoring, in: Proceedings of the Third World Congression on Engineering Asset Management and Intelligent Maintencance Systems, Beijing, China, 2008, pp. 1068–1076.
[27] X.M. Zhao, Q.H. Hu, Y.G. Lei, M.J. Zuo, Vibration-based fault diagnosis of slurry pump impellers using neighbourhood rough set models, Proceedings of the Institution of Mechanical Engineers, Part C: Journal of Mechanical Engineering Science 224 (2010) 995–1006.
[28] J.F. Gulich, Centrifugal Pumps, Spinger, New York, 2010.
[29] A. Muszynska, Rotor-to-stationary part rubbing contact in rotating machinery, in: Rotordynamics, CRC Press, 2005, pp. 555–709.
[30] G. Von Groll, D.J. Ewins, A mechanism of low subharmonic response in rotor/stator contact—measurements and simulations, Journal of Vibration and Acoustics 124 (2002) 350–358.
[31] G.X. Li, M.P. Païdoussis, Impact phenomena of rotor-casing dynamical systems, Nonlinear Dynamics 5 (1994) 53–70.
[32] H. Ma, T. Yu, Q. Han, Y. Zhang, B. Wen, C. Xuelian, Time–frequency features of two types of coupled rub-impact faults in rotor systems, Journal of Sound and Vibration 321 (2009) 1109–1128.